Atmospheric Research 132–133 (2013) 264–277

Contents lists available at ScienceDirect

Atmospheric Research

journal homepage: www.elsevier.com/locate/atmos

Surface electrostatic field below weak precipitation and stratiform regions of mid-latitude storms

S. Soula *, J.F. Georgis

Université de Toulouse/CNRS, LA (Laboratoire d'Aérologie), 14, avenue Édouard Belin - 31400 Toulouse, France

ARTICLE INFO

Article history:
Received 27 November 2012
Received in revised form 13 May 2013
Accepted 15 May 2013

Keywords:
Electrostatic field
Precipitation
Lightning
Thunderstorms

ABSTRACT

The electrostatic field is measured below thunderstorms at two sites in south-western France thanks to a field mill. It is recorded with a 1-s time resolution, simultaneously to the precipitation current measured with a specific sensor. The variations of both parameters are analyzed for two cases out of three storms considered in the study. Cloud-to-Ground (CG) lightning data from Météorage network and scans from a C-band radar included in the French network ARAMIS are used to characterize the storms. The magnitude of the electrostatic field can reach large values below the weak precipitation regions compared to the convective regions: between 5 and 6 kV m^{-1}, and between 2 and 3 kV m^{-1}, respectively. The field polarity is commonly negative (downward field) but it can reverse as the rainfall carries positive charge to the ground. So, the mirror effect is generally observed between the electrostatic field and the precipitation current. The electrostatic field magnitude can indicate the presence of large amounts of charge within the weak precipitation region above, although the lightning ground strokes remain relatively far. The fast field variations produced by CG flashes are analyzed. A strong dissymmetry for both CG polarities is observed: the +CG flashes can produce larger field discontinuities (~10 kV m^{-1}) even when their striking points are at about a distance of 40 km from the sensor, while the −CG flashes produce discontinuities lower than 4 kV m^{-1} even when the striking points are within 4 km around the sensor. This indicates that either the charge removed by a +CG flash can be horizontally displaced with respect to the ground stroke location, or it can be much larger compared to that removed by a negative CG flash. Our observations suggest the surface electrostatic field measured below these regions may provide valuable information for estimating local lightning risk.

1. Introduction

Stratiform precipitation may be associated with convection-generated cumulonimbus clouds (Houze, 1997). The thunderstorm systems where convective and stratiform regions coexist have generally lifetimes of a few hours. The stratiform precipitation develops within the older convection regions because of weak vertical air motions. Some of these systems can be classified as Mesoscale Convective Systems (MCS) if they are clusters of organized thunderstorm cells, at a scale of the order of at least 100 km. The shape of these systems can be round or linear and they can persist for many hours, much longer than the individual convective elements inside. Houze et al. (1990) identified symmetrical, asymmetrical and amorphous systems, based on the relative positioning of stratiform precipitation to the convective line, and the presence or absence of a linear convective region. Parker and Johnson (2000) expanded the terminology with trailing stratiform, leading stratiform, and parallel stratiform configurations.

Electrostatic field measurements from balloons have shown that the stratiform region consists of several layers of charge of alternating polarity. Marshall and Rust (1993) noticed that

* Corresponding author. Tel.: +33 561332774.
E-mail address: sous@aero.obs-mip.fr (S. Soula).

0169-8095
http://dx.doi.org/10.1016/j.atmosres.2013.05.008

profiles across different MCSs could be consistently categorized into two types: A, where five or six charge layers are more or less regularly distributed with height (also observed by Chauzy et al., 1985), and B, where two major oppositely charged layers reside near the melting level. In both types the charge around 0 °C was significant but opposite in polarity: for type B profiles, the charge layer near 0 °C tended to be narrow (250 m) and positive, while for type A, it tended to be negative. Stolzenburg et al. (1994) found a four-layer structure from electrostatic field soundings within the stratiform regions of several MCSs. The layers were horizontally extensive and ordered from up to down with a positive one probably formed by charge advected from the convective region, a negative one reinforced by noninductive processes, a positive one near 0 °C issued from in-situ charge mechanisms and a negative one like a screening layer. More recently, Stolzenburg et al. (1998) found up to six charge layers within the stratiform precipitation and the upper layers were issued from their counterparts in the convective region sloping downward toward the rear of the MCS. Several observations confirm the connection between the upper charge layers within the stratiform and convective regions (Stolzenburg et al., 1998; Carey et al., 2005).

Studies of the cloud-to-ground (CG) flash activity in MCS at various climatologic regimes (tropical, mid-latitude) showed a strong spatial relationship between their polarity/location and the distribution of the radar reflectivity. The −CG flashes usually are located in the region of higher radar reflectivity values that characterize the convective part of the MCS and the +CG flashes usually are essentially observed in the region of weaker radar reflectivity values associated with the stratiform portion of the MCS (e.g. in Rutledge and MacGorman, 1988; Rutledge et al, 1990; Petersen and Rutledge, 1992; Dotzek et al., 2005). On the other hand, the number of CG lightning flashes produced in the stratiform region is highly correlated with the vertical profile of the radar reflectivity (e.g. in Rutledge and Petersen, 1994). The +CG flashes in the stratiform region generally exhibit higher average peak currents than the other flashes (e.g. Rutledge and Petersen, 1994; MacGorman and Morgenstern, 1998; Dotzek et al., 2005). In parallel stratiform MCSs especially, +CG flashes have frequently been observed to concentrate near local reflectivity maxima (Parker et al., 2001; Rutledge et al., 1990). On the point of view of the total lightning activity, most flashes initiate within the convective line and propagate rearward within the stratiform region as observed by Lang and Rutledge (2008) for a asymmetric bow-echo MCS or by Carey et al. (2005) for a symmetrical MCS. Lightning flashes can initiate also within the stratiform region, generally close to larger reflectivity values associated with the mixed-phase region (Lang and Rutledge, 2008).

The surface electrostatic field and the precipitation current below the storm have been observed to follow evolutions that exhibit the mirror image effect (e.g. Ramsay and Chalmers, 1960; Moore and Vonnegut, 1977; Soula and Chauzy, 1997). This effect and the origin of the charge of the rain have been differently interpreted: (i) the charge of the raindrops is mainly positive (negative current) and due to the lower positive charge of the thundercloud tripole while the electrostatic field is positive (upwards) (Marshall and Winn, 1982). (ii) the charge of the raindrops originates from the capture of corona charge while they fall through the screening charge layer and the surface field is due to the approach of the positively charged rain (Wilson, 1929; Moore and Vonnegut, 1977). (iii) The rain carries the charge from the main cloud dipole, first negative (positive current) and then positive (negative current) in the case of a normal dipole. The surface electrostatic field reverses when the charge carried by the rain reaches the ground which leads to the mirror image effect (Soula and Chauzy, 1997; Soula et al., 2003).

The present study uses two types of data, from local measurement and from remote stations included in networks. The goal is to analyze the electrostatic field evolution below stratiform regions or low-reflectivity regions of three storms. The analysis is made in order to better understand the changes of the electrostatic field below these regions and to evaluate the usefulness of the electrostatic field for lightning warning. The data are defined in the second section of the paper and the following section is devoted to the description of the meteorological conditions of the considered storm events. Section 4 develops the results of the analysis of the parameters associated with the electrical activity. In Section 5 a discussion considers the main points in a general context. Finally the conclusion summarizes some features issued from the analysis.

2. Data and methodology

Fig. 1 displays the location of the study zone F (200 km × 200 km) in southwestern France and the main observation instruments. The surface measurement stations S_1 (43.129 N; 0.369E) and S_2 (43.187 N; 0.459E) include a field mill for the electrostatic field and a sensor for the precipitation current density. The latter has been described in Soula et al. (2003) and the principle of the measurement has been previously explained in Soula and Chauzy (1997). It consists of a 0.6-m high funnel-shaped conductor isolated and shielded with a 0.8-m high cylindrical tank covered with a grid connected to ground. Its shape is designed in order to avoid corona emission below thunderstorm electrostatic field conditions.

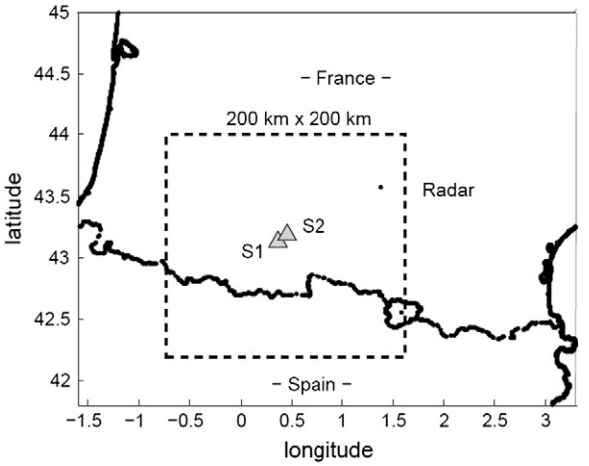

Fig. 1. Map of the experimental site in south-western France. The 200 km ×200 km frame F corresponds to the area in the following figures that display the radar reflectivity field. S_1 and S_2 show the location of both stations with electrostatic field and precipitation current measurement. The radar location corresponds to Toulouse.

The effective surface of the sensor corresponds to 0.2 m^2 and the current intensity measured is then converted in current density (A m^{-2}). This sensor can be slightly sensitive to other current components (currents of displacement, conduction, leakage because of humidity etc…) which can make a component independent of the rain. Thus, the interpretation of the data has to take into account these effects. The field-mill used in each station is of Previstorm type from Ingesco Company and initially used in Montanyà et al. (2009). Its measurement head is downward to avoid rain disturbances and it is fixed at the top of a 1-m mast that reinforces the electrostatic field on the measuring electrode. It has been cross-calibrated with another field mill flush with the ground (Soula et al., 2003). The result of the calibration is taken into account for the field values used in the study. According to this calibration and the maximum value that can be detected at the measuring electrode, the range of values is limited at about (−6.5 kV m^{-1}; 6.5 kV m^{-1}). The data from each sensor has been recorded with a time resolution of 1 s. This time resolution readily reveals the major discontinuities in the electrostatic field caused by the lightning flashes without the distracting effects of much faster individual processes within a flash. The polarity of the field is positive when it is created by negative charge overhead and that of the current is positive when negative charge move downward.

The polarity of the surface electric field measured in a unique location below complex charge structures indicates the sign of the charge that is the most efficient. Its evolution can indicate either a modification of the values of the charges within the structure or their displacement. It is therefore difficult to discuss the location and the polarity of the charge to interpret the electrostatic field recordings. The main study made from electrostatic field changes is the relationship with precipitation current and the analysis of discontinuities due to the CG flashes.

A lightning detection network provides location, polarity, peak current value, number of return strokes, and timing of CG lightning flashes. This network run by Météorage includes 18 sensors on French territory. All sensors use both magnetic direction finding (MDF) and time of arrival (TOA) techniques to determine the location of CG strokes (Cummins et al., 1998). The detection efficiency is ~90% over the French territory. Consecutive ground strokes are considered to belong to the same CG flash event provided they occur within 0.5 s and within 5 km.

The electrostatic field evolution is analyzed in order to identify discontinuities related to CG flashes. So, electrostatic field variations are calculated over 3-s intervals as follows:

$$\Delta E_f = E(t_2) - E(t_1) = E(t_f + 2 - \tau) - E(t_f - \tau - 1) \quad (1)$$

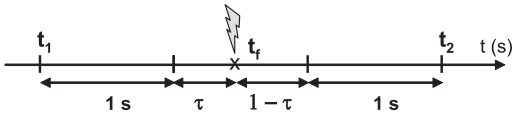

t_f is the time of detection of the ground stroke of the CG flash, τ is the time interval between t_f and the time of the precedent electrostatic field value reading. So, ΔE_f is calculated over a 3-s time interval surrounding the time of the CG flash detection t_f. The electrostatic field discontinuity ΔE_f is considered to be due to a flash when it is larger than 300 V m^{-1}. However, this value can be modified according to the case study, the activity of the storm in terms of electrostatic field evolution, and the possible noise in the signal. Finally there is not much ambiguity to identify flashes after considering the data carefully. When a flash signature is identified, it is considered corresponding to a CG flash if it is simultaneously detected by the lightning detection network, even if an IC component is possible (and generally connected to the CG channel). When no CG flash is simultaneously detected by the network, it is considered as a pure IC flash.

The C-band radar included in the French meteorological radar network ARAMIS (Application Radar à la Météorologie Infra-Synoptique) is located at about 100 km from S_1 (43.574 N; 1.376E). It provides data for the description of the structure of the storms. This radar has a range of approximately 250 km and it systematically produces Plan Position Indicator (PPI)-type images of the reflectivity factor every 5 min. Because of the low elevation of the radar beam in conventional mode, these images correspond to low altitude for the storm systems in the study area, typically between 2 and 4 km. The radar reflectivity factor Z used in the study is expressed in dBZ. The rainfall rate R is retrieved from Z by using the empirical Z–R relationship stemming from the Marshall and Palmer (1948) drop size distribution, generally used for precipitating systems in France:

$$Z_0 = 200\, R^{1.6}$$

where R is in mm h^{-1}, Z_0 is in mm m^{-3} and proportional to the density of particles n and their diameter D ($Z_0 \propto n\, D^6$) in the volume scanned by the radar beam, and Z_0 is related to Z by a logarithm law:

$$Z = 10 \log Z_0$$

Marshall–Palmer law was found to be a reasonable approximation for average conditions and generally used for mid-latitude weather systems (Salek et al., 2004).

3. Overview of the events

3.1. Synoptic situation

The 500 hPa geopotential and wind based on the National Centre for Environmental Prediction analyses are presented in Fig. 2a–c, at 1200 UT for 28 June, 19 July and 7 September 2006, respectively. The synoptic situation prevailing at 1200 UT on 28 June is characterized by the presence at 500 hPa of a trough located 27° west of Ireland and an anticyclone area extending from north of Africa to south of Italy. At 1200 UT on 19 July, a similar situation is observed but the locations of the trough and the anticyclone area are slightly shifted to the south and to the southwest, respectively. As a consequence, the geopotential gradient is stronger over Spain and western part of the Pyrenees range and the associated cyclonic southwesterly flow is necessarily more intense. Surface wind bursts higher than 100 km h^{-1} are thus observed in southwestern France during the afternoon. At 1200 UT on 07 September, Spain and southern France are again under influence of an

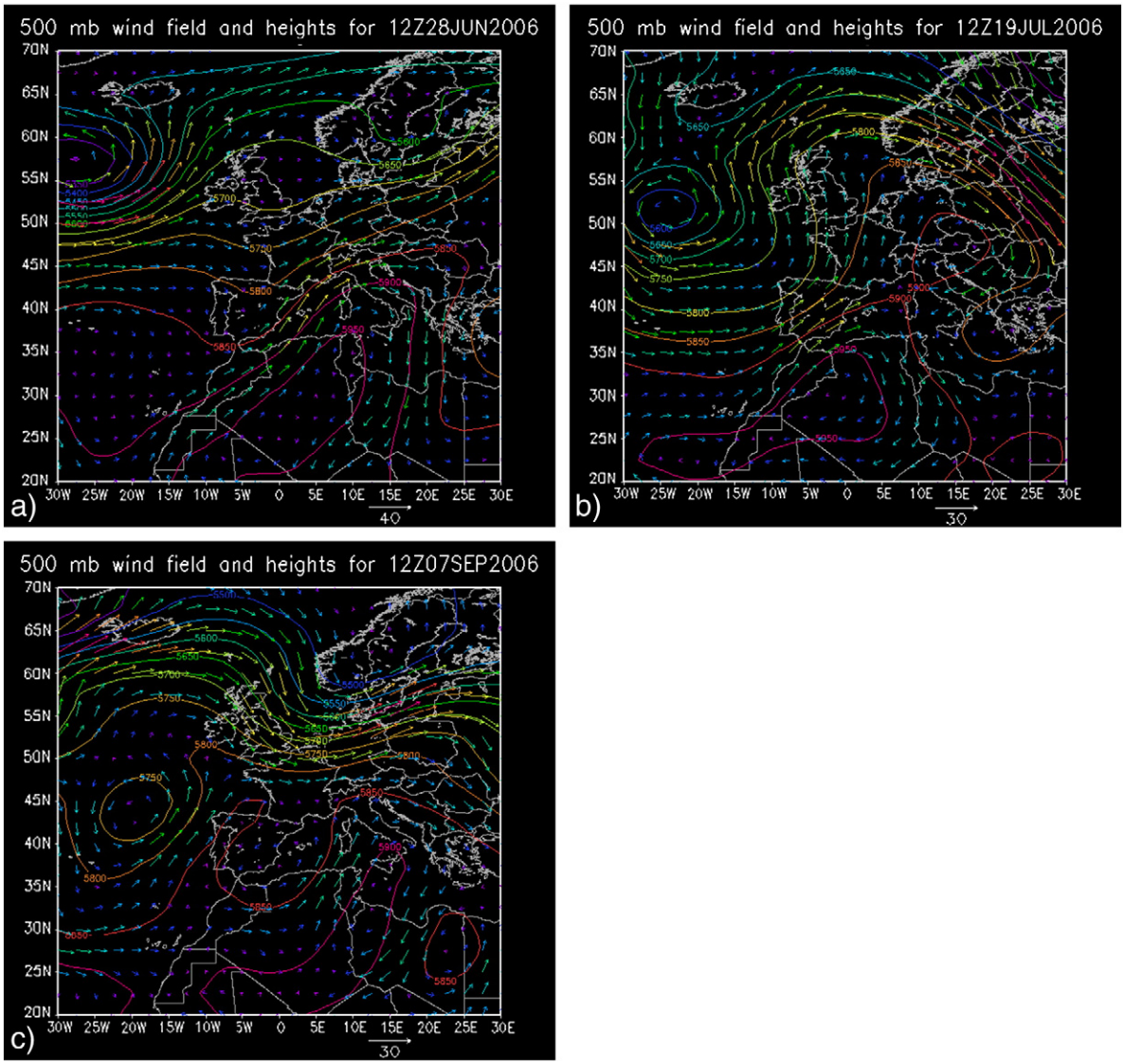

Fig. 2. 500 hPa geopotential height (contours every 50 m) and wind vectors (reference vector in downer–right corner in m s^{-1}) at: (a) 1200 UT on 28 June, (b) 1200 UT on 19 July, (c) 1200 UT on 7 September 2006, from the National Centers for Environmental Prediction analyses.

anticyclone extending from north of Africa to south of Italy but the trough observed over the Atlantic Ocean west of Ireland during the two previous events is then located more southerly (at the latitude of Pyrénées range) and, especially, is much more moderate. Also, the 500 hPa geopotential field is much more uniform over Spain and southern France and, consequently, the air flow is highly reduced in the Pyrenean regions.

3.2. Mesoscale characteristics

In order to roughly estimate the mesoscale characteristics of the environmental flow during the three considered events, we use data from radiosoundings launched at Bordeaux Merignac (44.83 N; 0.7 W) about 200 km north-west of the study zone (shown in Fig. 3) and at Zaragoza (not shown). These soundings are the closest (200 km) upstream and downstream, according to the event. For all the situations, according to Bordeaux Merignac radiosoundings, the environmental flow is characterized by low moisture at every altitude with a minimum relative humidity at 500 hPa, 400 hPa and 600 hPa on 28 June, 19 July and 7 September respectively. Except at the lowest levels, the atmosphere is systematically moister at Zaragoza with a maximum relative humidity (higher than 80%) at around 500 hPa. Although the level of free convection (LFC) is systematically lower in France, the energy per unit mass required to lift a negatively buoyant air parcel from the surface to the LFC (convective inhibition, CIN) is always higher than 90 J kg^{-1}. Due to a low-level inversion, such a high CIN indicates a strong low-level thermodynamic stability. Deep convection is then unlikely to occur in the absence of external forcing. Strong uplift of this layer is thus needed to release the convective instability. This is probably achieved when the south-westerly airflow impinged on the Pyrénées range on 28 June (Fig. 2a) and 19 July (Fig. 2b) as already observed during

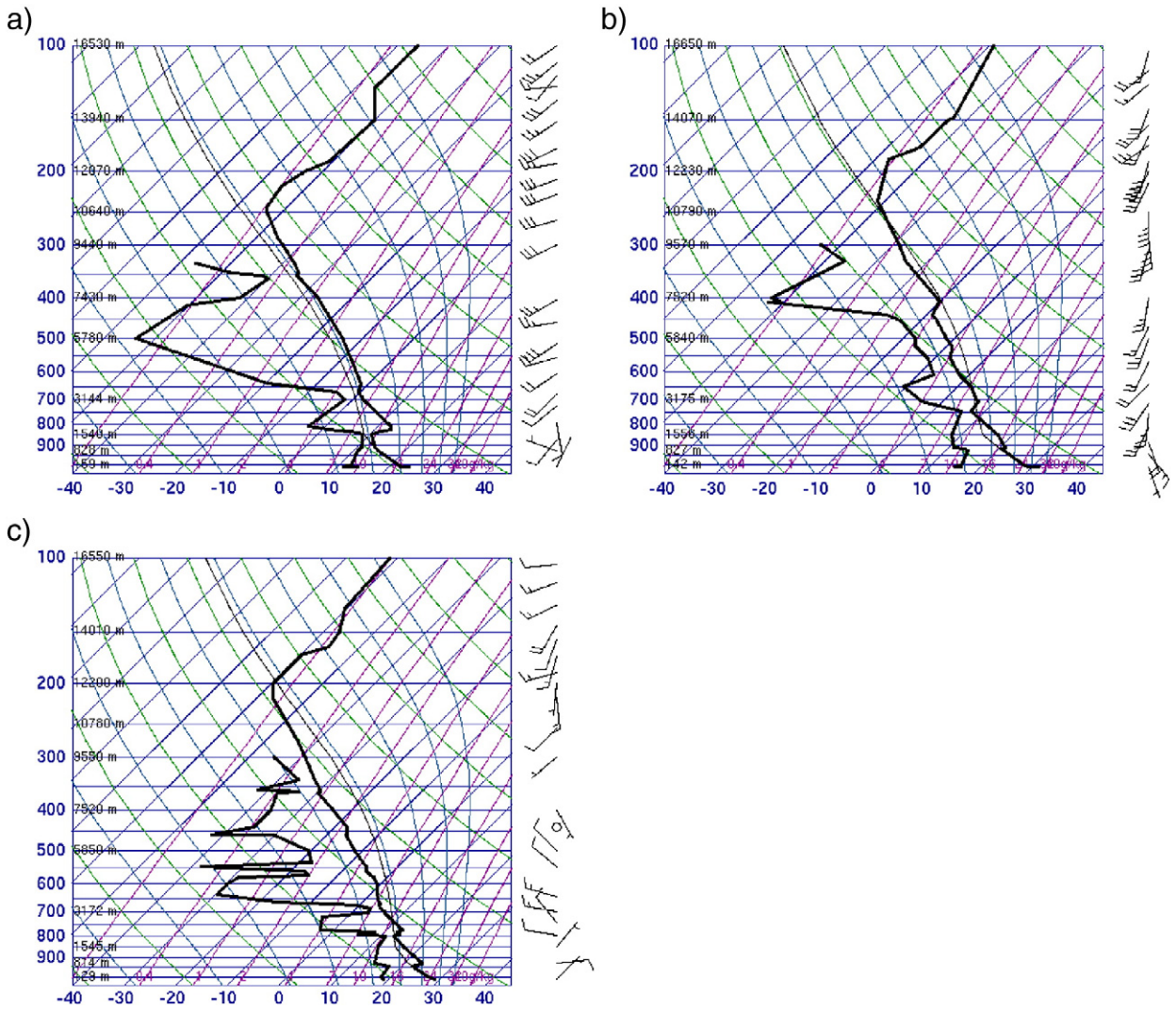

Fig. 3. Skew T–Log pdiagrams from radiosoundings launched at Bordeaux Merignac (a) at 1200 UT on 28 June 2006; (b) at 1200 UT on 19 july 2006; (c) at 1200 UT on 7 September 2006. Wind barbs display both wind speed and direction at various altitude. Full barbs are 10 knots and half barbs are 5 knots. Barbs point the direction the wind is coming from (for example, in Fig. 3a, wind above the 800 hPa level is from the southwest).

the Mesoscale Alpine Program campaign in another mountainous area (Georgis et al., 2003). However, the convective instability is moderate for these two situations since the CAPE, i.e. the energy per unit mass that can be released through buoyancy from the LFC up to the equilibrium temperature level, is slightly lower than 450 J kg^{-1}.

On 7 September, the convective instability is stronger since the CAPE deduced from the Bordeaux Merignac radiosounding data is higher than 1450 J kg^{-1}. This time, the release of this stronger convective instability is probably favoured by the northerly surface wind toward the Pyrenean barrier (not shown). Conditions are thus propitious to orographic precipitation on the northern slopes of the Pyrénées range. This scenario is consistent with the Zaragoza radiosounding data (not shown) since the lowest atmosphere (below 3000 m altitude) appears drier at Zaragoza south-side of the Pyrenees range.

4. Electrical activity of the case studies

4.1. 28 June, 2006 – Multicell storm

On 28 June 2006, a multicell storm system develops over northern Spain and moves north-eastward relatively quickly (~40 km h^{-1}). Fig. 4 displays the location and the structure of the storm system thanks to the radar reflectivity field and the location of the CG flashes, at different times of its evolution (1400, 1420, 1445 and 1515 UT for a, b, c and d, respectively) in the frame F of Fig. 1, centered on S_2. The CG flashes produced during 10 min around the time of the radar scan are plotted in each graph. At 1400 UT (Fig. 4a) the main storm system is located at a distance lower than 50 km south of S_2 with some active cells spreading to the east. The maximum reflectivity factor is about 60 dBZ in the most westerly convective region of the system and around 55 dBZ in

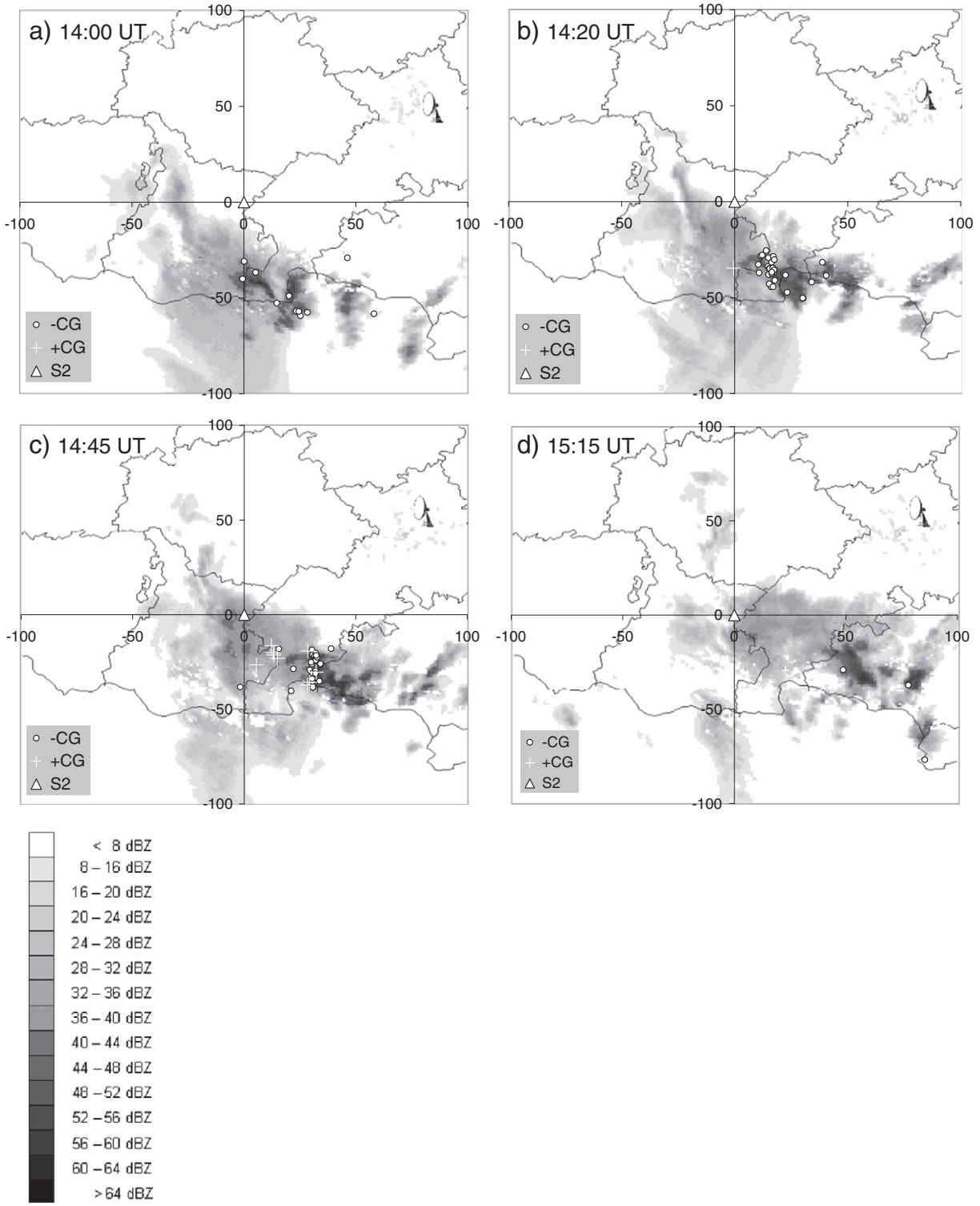

Fig. 4. Event on June 28th. Chart of the radar reflectivity in F at (a) 1400 UT, (b) 1420 UT, (c) 1445 UT and (d) 1515 UT. Plus (dots) indicate the +CG (−CG) flashes detected during 10 min around the time of the radar scan.

the other cells. Only −CG flashes are detected between 1355 and 1405 UT and they are located close to the convective cores.

Fig. 5 displays the evolution of the surface electrostatic field and the precipitation current density. It shows also the distance of the CG flashes (−CG and +CG) detected in a

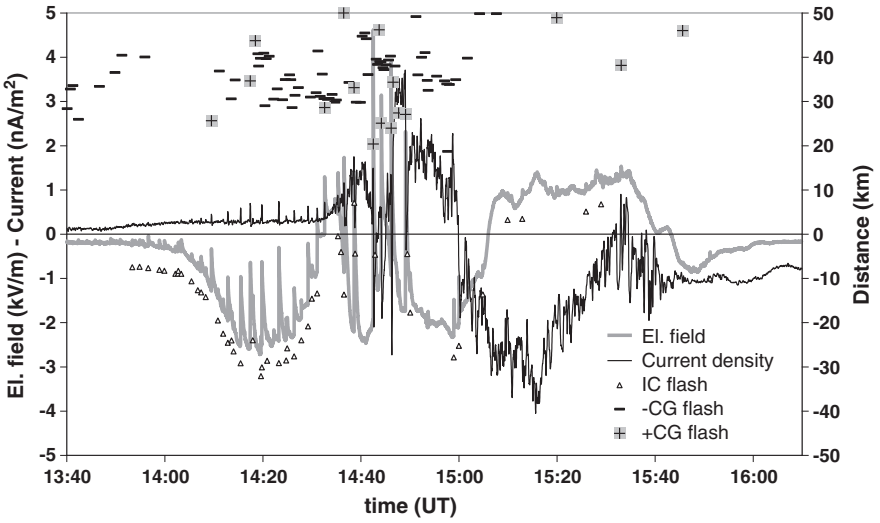

Fig. 5. Event on June 28th. Time series of the electrostatic field and the precipitation current density measured in S_2. The symbols (+) and (−) indicate the distance to S_2 of the +CG and −CG flashes, respectively, detected by Météorage. The symbols (Δ) plotted below the electrostatic field curve indicate IC flashes that could be at the origin of a visible field discontinuity.

radius of 50 km around S_2. The surface electrostatic field is negative at the beginning of the period considered in the graph (1340 UT). This polarity is that of the fair weather and the absolute value at that time is about 0.2 kV m $^{-1}$, i.e. slightly larger than the typical fair weather field. The trend of the electrostatic field magnitude is to increase progressively until ~ 1420 UT when it reaches a maximum value and then decreases as the system approaches and moves above S_2. This first sequence in the electrostatic field evolution indicates the field is created by a net positive charge that is approaching the measurement station S_2. This positive charge may be in the upper part of the cloud that is at a few kilometers of distance at that moment according to Fig. 4a and b. Furthermore, several discontinuities in the time series of the electrostatic field show that lightning flashes are produced. They correspond to decreases in absolute value, i.e. the net positive charge producing the electrostatic field is partially neutralized by these flashes. For most of these discontinuities no CG flash is detected and therefore they are probably due to IC flashes as indicated in Fig. 5 with symbols (Δ). However, a +CG flash detected by the system produces a visible discontinuity at 14 h 17 min 26 s. In that case the +CG flash is detected at 35 km south from S_2 (visible in Fig. 4b) and its peak current is 36 kA.

Fig. 4b displays the reflectivity field at 1420 UT and the CG flashes detected between 1415 and 1425 UT. This radar scan shows that the edge of the precipitating system arrives above S_2 while the electrostatic field reaches its maximum in negative value (~ −2.5 kV m^{-1}) around 1420 UT. Then, the electrostatic field magnitude decreases while the precipitating system moves above S_2, and reverses at about 1432 UT. The precipitation current increases in positive value after 1432 UT, i.e. negative charge is carried to the ground by raindrops and simultaneously the electrostatic field recovered a negative polarity for a few minutes. The approach of this negative charge, probably located at a lower height than the positive charge leading to the initial negative polarity of the electrostatic field, can explain the decrease of the electrostatic field in absolute value after 1420 UT. When the rainfall carries this negative charge to the ground after 1430 UT, the electrostatic field recovers larger values in negative polarity. Thus, a short sequence of a few minutes (1433–1442 UT) clearly exhibits the mirror image effect between electrostatic field and precipitation current.

Fig. 4c displays the reflectivity field at 1445 UT and the CG flashes detected between 1440 and 1450 UT. At that moment the maximum reflectivity factor is much larger in the eastern part of the system compared to its western part, 60 dBZ and 44 dBZ, respectively. The western part looks like a stratiform region moving besides a convective region, which could correspond to a parallel stratiform MCS (Parker and Johnson, 2000). Five +CG flashes are detected in a south-east direction between 20 and 27 km from S_2. They exhibit peak current values ranging from 11.5 to 34 kA. These +CG flashes produce large electrostatic field "jumps" visible in Fig. 5. They lead to positive field values (upward electrostatic field, i.e. produced by a net negative charge). Fig. 4c shows they are located within the stratiform-like region of the storm with radar reflectivity values lower than 40 dBZ. According to the large field discontinuities observed, we can suppose that large amounts of positive charge are neutralized in the cloud by these flashes and that a substantial proportion of this charge is located relatively close to S_2, even if the +CG strokes are located far from S_2 (more than 20 km).

The polarity of the electrostatic field between 1435 and 1500 UT corresponds to that created by a positive charge and the +CG flashes neutralize part of this charge. The precipitation current density exhibits positive values (negative charge going down) between 1442 and 1500 UT with a very clear mirror effect. Then, its polarity reverses around 1500 UT and the electrostatic field decreases simultaneously in absolute value to reverse its polarity 6 min later at 1506 UT. Thus, the rain detected in S_2 first carries negative charge

and then positive charge. The mirror image effect between electrostatic field and precipitation current is observed for a few tens of minutes. Fig. 4d shows the radar reflectivity at 1515 UT is low above S_2 (~25 dBZ) and corresponds to very light rain while a small core of reflectivity exceeding 40 dBZ is located southeast at a distance of ~10 km. A −CG flash

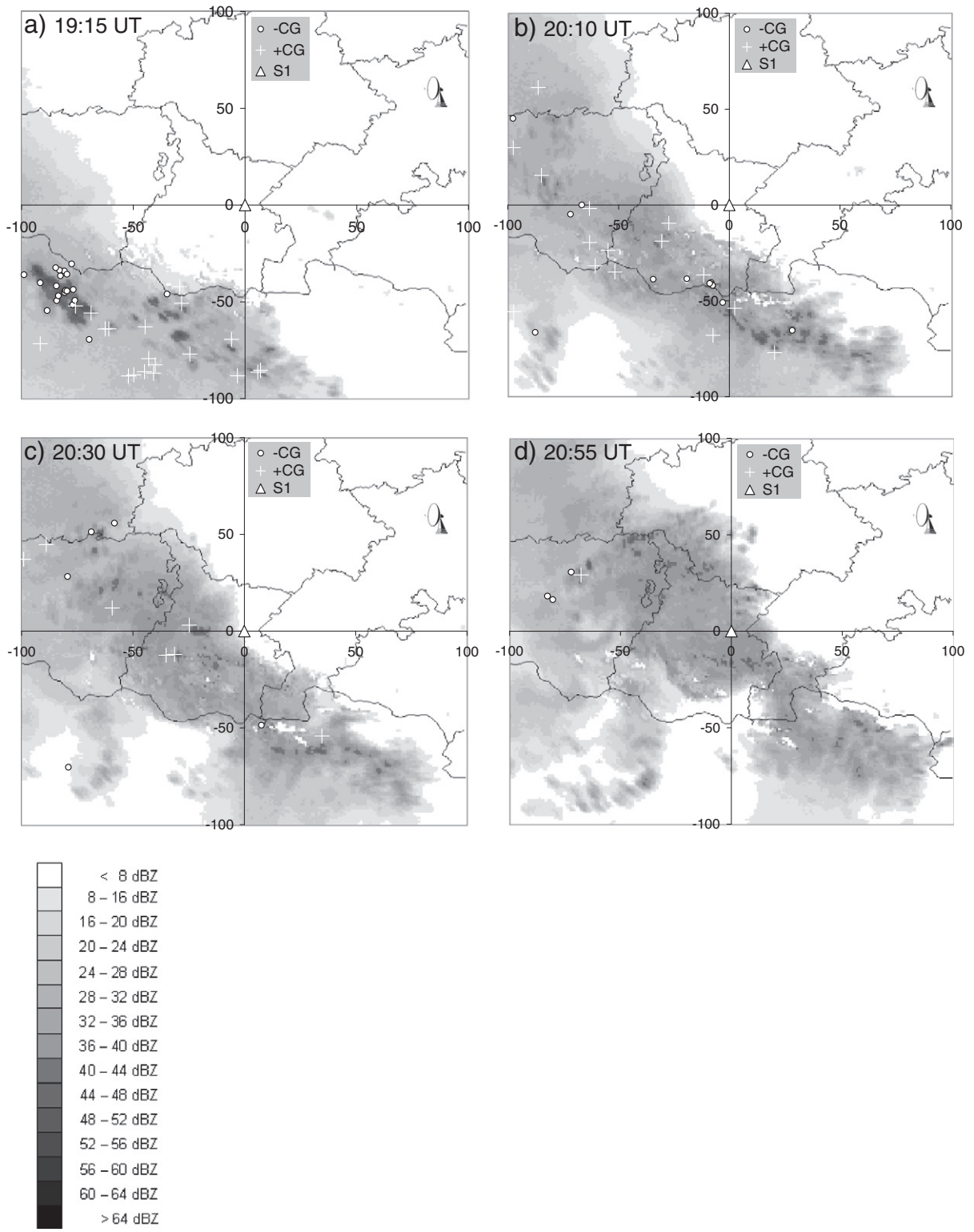

Fig. 6. Event on July 19th. Chart of the radar reflectivity in F at (a) 1915, (b) 2010, (c) 2030 and (d) 2055 UT. Plus (dots) indicate the +CG (−CG) flashes detected during 15 min around the time of the radar scan.

detected during this period at 14 h 57 min 47 s at a distance lower than 20 km produces no visible field discontinuity at that moment. The end of the field evolution after 1500 UT is typical of the end-of-storm-oscillation (EOSO). The CG flashes detected after 1500 UT are located at more than 30 km and do not produce any visible signature on the electrostatic field evolution.

4.2. 19 July 2006 – Dissipating storm

Fig. 6 displays the radar reflectivity field in the 200 km × 200 km area centered on S_1 on 19 July at 1915, 2010, 2030 and 2055 UT, for a, b, c, and d, respectively. It displays also the location of the CG flashes produced during 15 min around the time of the radar scan. A large west-northwest/east-southeast-oriented cloud system is located above the French–Spanish border in the evening and Fig. 6 shows a small part of it. At 1915 UT the edge of the precipitating system including several convective cells is located south of S_1 at a distance of ~50 km as indicated in Fig. 6a. Some convective cells embedded in the whole system, exhibit reflectivity values lower than 54 dBZ for the biggest one in the west part of the graph, and lower than 50 dBZ for most of them. The main convective cell is at a decaying stage and was more active a few tens of minutes earlier. On the contrary, the small cells located in the eastern part of the system are being developed at that time. Several −CG flashes are produced in the largest convective region while some +CG flashes are produced in a large area of the system. At 2010 UT (Fig. 6b) the edge of the precipitation detected by the radar is maintained at a distance of 20 km from S_1. The main convective region visible in Fig. 6a has disappeared within the cloud system which means it is in dissipating stage. The largest values of the reflectivity (49 dBZ) are located in several small convective cells in the eastern cloud region. The precipitation approaching above S_1 is light with reflectivity values lower than 36 dBZ.

Fig. 7 displays the time series of the surface electrostatic field and the precipitation current density measured in S_1. The electrostatic field increases in positive value until 2015 UT and exhibits some flash signatures, corresponding to small increases due to IC and +CG flashes. No −CG flash signature is visible. The +CG flashes that affect the electrostatic field (one at 20 h 04 min 43 s and one at 20 h 11 min 23 s) are located southwest at a distance of 30–40 km from S_1. The electrostatic field reverses rapidly to negative values (created by a net positive charge overhead) around 2025 UT and remains negative for approximately one hour, except for an excursion to positive values that begins around 2042 UT and lasts approximately 7 min (Fig. 7).

Radar reflectivity at 2030 UT (Fig. 6c), during the initial period of negative polarity of electrostatic field, shows a broad region of stratiform precipitation arriving above the field mill. Three +CG flashes that produce large field discontinuities between 2028 and 2034 UT are located at a distance from S_1 of 25, 37, and 33 km, respectively, and exhibit peak current values of 115, 12, and 35 kA, respectively. A core of reflectivity between 40 and 46 dBZ appears at a distance of 20 km west of S_1 and produces one of the +CG flashes, while the largest field change is produced by a +CG flash at a distance of 33 km from S_1 and at the edge of a small core of reflectivity larger than 40 dBZ. The precipitation current exhibits larger and larger negative values after 2042 UT and the magnitude of the negative electrostatic field simultaneously decreases, and then reverses at about 2048 UT. The ~7-min excursion of the electrostatic field to positive values (around 2053 UT) coincides with the increase in absolute value of the negative precipitation current (lowering positive charge to the ground) that reaches a minimum value of about −5 nA m^{-2} at 2055 UT. The excursion of the electrostatic field ends as the precipitation current magnitude decreases rapidly to near zero. No flash signature is visible in the electrostatic field during or after this excursion, and all CG flashes are at a distance larger than 60 km from S_1. The chronology observed between 2000 and 2100 UT in Fig. 7 seems to roughly indicate the approach of an inverted charge dipole in the stratiform-like cloud system (negative charge above positive charge). As a matter of fact, the electrostatic

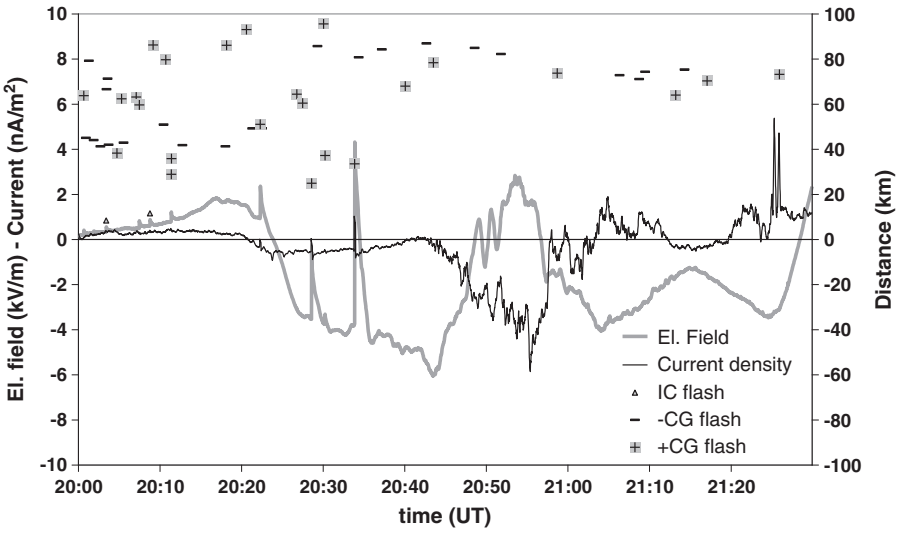

Fig. 7. Event on July 19th. Same as Fig. 5 for the electrostatic field and the precipitation current measured in S_1.

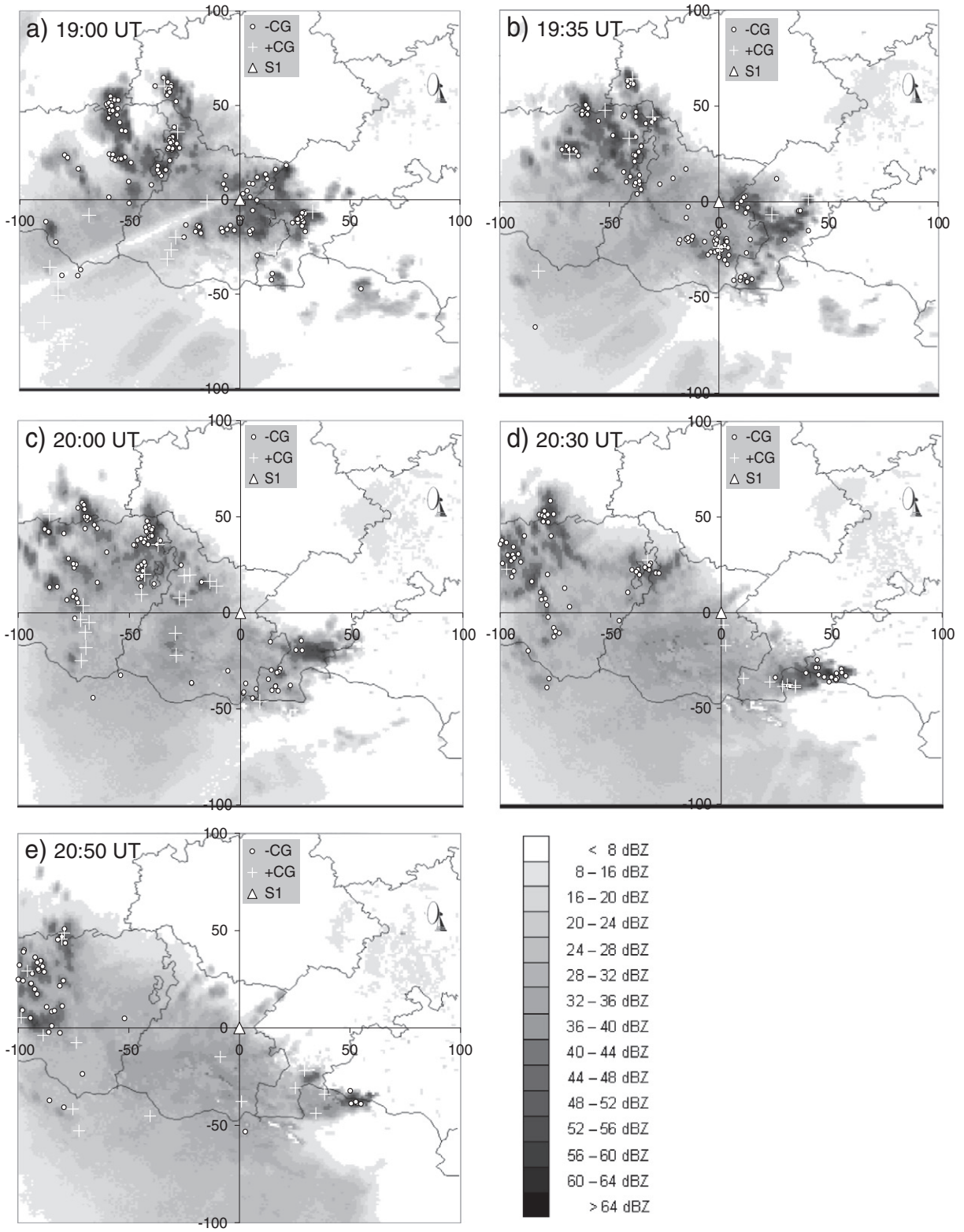

Fig. 8. Event on September 7th. Chart of the radar reflectivity in F at (a) 1900, (b) 1935, (c) 2000, (d) 2030 and (e) 2050 UT. Plus (dots) indicate the +CG (−CG) flashes detected during 10 min around the time of the radar scan.

field exhibits first low values mainly due to the effect of a negative charge and then it reverses rapidly to negative polarity, under the effect of a positive charge, to reach larger values in absolute value. This positive charge seems to reach the ground carried by the rain between 2045 and 2100 UT.

4.3. 7 September 2006 – MCS with trailing stratiform region

A very active storm system approaches S_1 in the afternoon on 7 September and the biggest convective core arrives above it at about 1830 UT. Fig. 8 displays the radar reflectivity field and the CG flashes at selected times of the activity of this storm system (1900, 1935, 2000, 2030, and 2050 UT for a, b, c, d, and e, respectively). The CG flashes produced during 10 min around the time of the radar scan are plotted in each graph. We can note radial deficits in reflectivity due to attenuation of C-band radar signals by heavy rain, especially in Fig. 8a and b. Fig. 8a shows S_1 is below the west edge of a large convective region of the storm at 1900 UT. The highest radar reflectivity values (~58 dBZ) are observed in the eastern part of this region while the western part exhibits lower values (~52 dBZ). According to the law from Marshall and Palmer (1948), the rain rates corresponding to these values are ~150 mm h^{-1} and 50 mm h^{-1}, respectively. Thus, the rain rate is so large above S_1 that the sensors at the ground are strongly disturbed for the measurement during a few tens of minutes (highly wet air, water splashing…). After 1900 UT the convective core splits in three parts, two of which moves southward. At 1935 UT, the third one is located east of S1 at a distance of 10 km, as indicated in Fig. 8b. It exhibits a maximum reflectivity value around 50 dBZ and it produces −CG flashes at that moment.

Fig. 9 displays the time series of the electrostatic field and the distance of the CG flashes detected within 50 km around S_1, between 1930 and 2130 UT. During the first 10 min of the sequence the electrostatic field evolves as if produced by a negative charge above with discontinuities due to flashes. Some of these flashes are identified as −CG flashes by Météorage and other are probably IC flashes. The core of reflectivity located south of S_1 at a distance of 20 km, produces a large amount of −CG flashes at that moment, while the reflectivity does not exceed 48 dBZ.

At 2000 UT (Fig. 8c) the overall storm system consists of several convective cells in its western part and a convective core in its eastern part, both with a maximum reflectivity value around 60 dBZ, separated by a stratiform region with reflectivity values lower than 40 dBZ. The electrostatic field is positive, i.e. due to a dominant negative charge overhead. The large field discontinuities are due to +CG flashes (19 h 55 min 30s, 19 h 58 min 51 s, 20 h 01 min 18 s for example) that are detected at a distance from S_1 of 21.5, 28.5 and 30 km, respectively, and that exhibit peak currents of 51, 22, and 41 kA, respectively. Other field discontinuities are due to IC flashes (20 h 02 min 55 s for example). The surface electrostatic field reverses at about 2020 UT, then rapidly reaches negative values around −5 kV m^{-1} and exhibits some large discontinuities due to +CG flashes that are detected by Météorage. For example, three of them that are produced between 2025 and 2035 UT (Fig. 8d) are located at a distance from S_1 of 17, 36, and 7 km, respectively. Even that detected at 36 km (with a peak current of 49 kA) produces a large field jump (6 kV m^{-1}) at 20 h 31 min 32 s. At 2030 UT (Fig. 8d) the stratiform region of the storm is strongly extended (~70 km) between both convective regions and still over S_1, and it is even larger at 2050 UT as indicated in Fig. 8e. Large field discontinuities observed in Fig. 9 at 20 h 37 min 37 s, 20 h 40 min 08 s, and 20 h 48 min 02 s are associated with +CG flashes detected at a distance from S_1 of 13, 42, and 40 km, respectively, with peak current values of 37, 43, and 12 kA, respectively. The electrostatic field recovers rapidly its initial value after each discontinuity while it progressively decreases in absolute value after 2040 UT. Thus, except for some reverses due to flashes, it stays negative during about 50 min before reversing definitely positive at 2110 UT. This last reverse corresponds with the cloud movement away, which signifies a larger influence of negative charge at that moment.

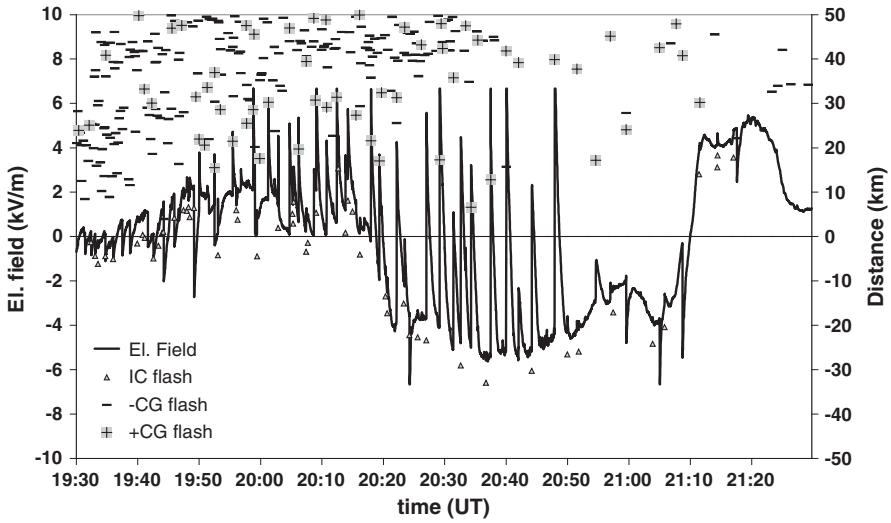

Fig. 9. Event on September 7th. Same as Fig. 7 for the electrostatic field measured in S_1.

5. Discussion

The precipitation current has been measured simultaneously to the electrostatic field in two out of the three cases of storm. In both cases it reaches a few nA m^{-2} in both negative and positive polarities and it can reverse its polarity during the rainfall. Its changes are clearly linked with those of the electrostatic field. When the precipitation current increases, the electrostatic field generally starts to decrease in absolute value: if the rainfall carries negative charge (positive current), the electrostatic field evolves into negative (dominant positive charge overhead) and conversely if the rainfall carries positive charge (negative current), the electrostatic field evolves into positive (dominant negative charge overhead). According to the present observations, the electrostatic field reverses after the precipitation current is detected, with a delay that can reach several minutes, and the mirror image effect is then observed. This behavior may take several tens of minutes and is observed in several sequences issued from both Fig. 5 (1433–1500 UT; 1500–1530 UT) and Fig. 7 (2043–2058 UT; 2102–2112 UT). However, it is not always observed at the end of the storm activity recorded, (2124–2130 UT in Fig. 7). Thus, most sequences of precipitation current confirm previous observations by Soula et al. (2003) for different kinds of convective cells. The same observation is made below the weak precipitation region of storms in the present case. It can be interpreted by saying the precipitation carries charges from the cloud that created the surface electrostatic field before rainfall. When this charge reaches the surface, the electrostatic field decreases and then reverses. In the present cases, the rainfall issued from weak precipitation regions can carry positive or negative charge. In one case, the charge is first negative and then positive, and in the other case the opposite. It seems the arrival of the rain charge of a given polarity at the ground can depend on the location of the system with respect to the measurement site. It is not surprising to detect both types of charge carried by the rainfall originated from weak precipitation regions, according to the multi layer-structured charge observed by sounding (e.g. Stolzenburg et al., 1994, 1998) and previous observations of charge of both polarities from soundings by balloon crossing rainfalls below thunderclouds (Marshall and Lin, 1992).

The electrostatic field can exhibit large values (5 to 6 kV m^{-1}) below the stratiform region or the storms at dissipating stage when the lightning flash rate is low, while it ranges between 2 and 3 kV m^{-1} when the convective region is closer and the flash rate is high. For storms in Florida, Livingston and Krider (1978) find also larger values (2–4 times) of the time- and area-averaged surface electrostatic field when the flash rate is lower at the end of storm lifetime. The third storm (7 September) of the present study provides a good example of this behavior. Below the stratiform region of this storm, the electrostatic field reaches large values by exhibiting an evolution characteristic of the point discharge effect at the ground: rapid recoveries after large discontinuities due to lightning flashes and "stabilizations" between lightning flashes as previously described by Standler and Winn (1979), Krider and Musser (1982), Chauzy and Soula (1987) and Soula (1994). The mechanism that is put forward to explain this observation is related to the point discharge: the ions produced at the surface (corona ions) rise rapidly and form a screening charge layer that limits the surface electrostatic field because their production rate increases rapidly with the electrostatic value.

Fig. 10 displays the values of the field discontinuities ΔE_f calculated according to (1) versus the detection distance for CG flashes of both polarities. The distribution is limited to CG flashes detected at a distance lower than 50 km around the field sensor. CG flashes considered in the graph are issued from the three storm events: 86, 15, and 256 CG flashes for 28 June, 19 July, and 7 September, respectively. Among these CG flashes, 288 are − CG and 69 + CG. The distance is considered ~~as~~ negative for the − CG flashes in order to distinguish the

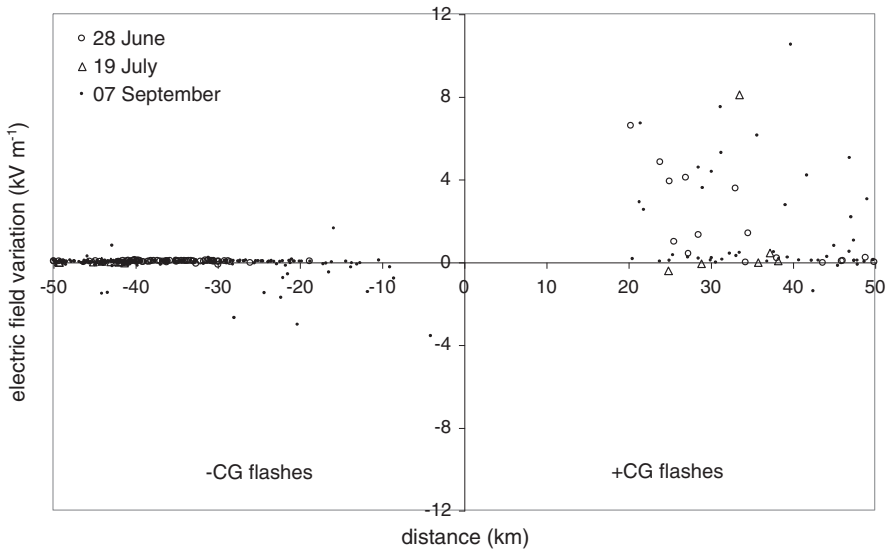

Fig. 10. Distribution of value of the electrostatic field discontinuity ΔE_f versus the distance of detection of the CG flash that produces it. The CG flashes from three events are mixed.

two polarities in the graph. The distribution is very different for +CG and −CG flashes. 25 +CG flashes (36%) produce ΔE_f values larger than 1 kV m^{-1} and only 8 −CG flashes (2.8%). The maximum value of ΔE_f is 10.5 kV m^{-1} for the +CG flashes (for a flash detected at about 40 km) and only 3.6 kV m^{-1} (in absolute value) for the −CG flashes (for a flash detected at about 4 km). All −CG flashes producing substantial values of ΔE_f correspond to the event of 7 September. For a given value of their detection distance, +CG flashes can produce varying ΔE_f values. The ΔE_f value depends on the amount and the location with respect to the field mill, of the charge involved in the discharge process. If the ΔE_f value is large we can think that either part of the charge neutralized by the CG flash in the cloud region is relatively close to the field measurement station, or it is large. In the present study, even if the stroke of a +CG flash is detected far from the field mill it can produce a large ΔE_f. Several interpretations can be advanced: (i) Since the lightning flashes can propagate over large distances in the stratiform region (Mazur et al., 1998; Lang et al., 2004; Carey et al., 2005; Lang and Rutledge, 2008 and others), the region concerned by the discharge can be located above the measurement site if the path of the flash travels in its direction from the triggering point. In this case the electrostatic field value provides information about the presence of charge above and therefore about lightning warning, even when no CG flash is detected at a short distance. (ii) The +CG flash is very efficient to neutralize a large amount of charge within the cloud, especially thanks to a continuous current after the return stroke (Rakov et al., 1994; Ferro et al., 2009). On the other hand, the literature shows the +CG flashes exhibit larger peak currents (Orville and Huffines, 1999; Fleenor et al., 2009) and they are generally more destructive (Aranguren et al., 2009).

The cases documented and presented in this paper show that both charge polarities can be carried by the rainfall issued from stratiform or weak precipitation storm regions and generally, they follow each other during the precipitation sequence. For the CG lightning flashes, it appears that the positive ones are much more frequent in these regions. The origin of the charge located inside the stratiform region of the storm is a question that has been discussed in many studies. Several works show a large proportion of the charge in the stratiform region is issued from in-situ non-inductive charging processes: Rutledge and Houze (1987) found that updrafts are responsible for 80% of the charge in the stratiform region; Schuur and Rutledge (2000) tested different mechanisms by modeling and found that 70% of this charge could be produced within the updrafts for a trailing stratiform (TS)-MCS. According to the strong dissymmetry observed for the ΔE_f values produced by CG flashes of both polarities (Fig. 10), the positive charge neutralized by the +CG flashes is probably much larger than the negative charge neutralized by the −CG flashes.

6. Conclusion

Several electrical parameters recorded during three storm events are analyzed in order to better interpret the variations of the electrostatic field measured below the stratiform region of thunderstorms. CG lightning flashes detected by the French detection system managed by Météorage Company, precipitation current density detected with a specific sensor simultaneously to the electrostatic field, and PPI-type radar scans issued from C-band radar included in the French radar network ARAMIS are considered in this study. Especially, the distance of the CG flash is compared to the field discontinuity involved by the CG flash, by taking into account the CG flash polarity. The radar scans allow characterizing the region of the storm above the electrostatic field and precipitation current sensors. Some observations that can be considered as new findings in the knowledge of the electrical processes associated with the storm are summarized as follows:

(i) The electrostatic field magnitude reaches larger values below the stratiform region compared to below the convective region. During its slow variations, it reaches 5 to 6 kV m^{-1} below the stratiform region, while below the convective region of a very active storm it is observed between 2 and 3 kV m^{-1}.
(ii) The field polarity is more often negative (downward field produced by a dominant positive charge overhead) below the stratiform region. When the rainfall carries charge to the ground, the electrostatic field undergoes a decrease and reverses its polarity which generally involves a mirror effect between the electrostatic field and the precipitation current.
(iii) The electrostatic field magnitude can indicate the presence of large amounts of charge within the cloud above a site although the lightning ground striking points remain relatively far. This observation can support the usefulness of the electrostatic field detection for warning of a risk for local lightning stroke.
(iv) A strong dissymmetry is observed for the variations of the electrostatic field amplitude induced by −CG and +CG flashes: the +CG flashes can produce a large field discontinuity (~10 kV m^{-1}) even when its distance is about 40 km while the –CG flashes considered in the study produce a maximum discontinuity of –3.6 kV m^{-1} at a distance of 4 km. It indicates either the charge removed by a +CG flash can be horizontally displaced compared to the ground stroke location, or it can be larger thanks to more efficient processes (continuous current component for example).

References

Aranguren, D., Montanya, J., Sola, G., March, V., Romero, D., Torres, H., 2009. On the lightning hazard warning using electrostatic field: analysis of summer thunderstorms in Spain. J. Electrost. 67 (2–3), 507–512. http://dx.doi.org/10.1016/j.elstat.2009.01.023.

Carey, L.D., Murphy, M.J., McCormick, T.L., Demetriades, N.W.S., 2005. Lightning location relative to storm structure in a leading-line, trailing-stratiform mesoscale convective system. J. Geophys. Res. 110, D03105. http://dx.doi.org/10.1029/2003JD004371.

Chauzy, S., Soula, S., 1987. General interpretation of surface electric field variations between lightning flashes. J. Geophys. Res. 92 (D5), 5676–5684.

Chauzy, S., Chong, M., Delannoy, A., Despiau, S., 1985. The June 22 tropical squall line observed during the COPT 81 experiment: electrical signature associated with dynamical structures and precipitation. J. Geophys. Res. 90, 6091–6098.

Cummins, K.L., Murphy, M.J., Bardo, E.A., Hiscox, W.L., Pyle, R.B., Pifer, A.E., 1998. NLDN'95, A combined TOA/MDF technology upgrade of the US National Lightning Detection Network. J. Geophys. Res. 103, 9035–9044.

Dotzek, N., Rabin, R.M., Carey, L.D., MacGorman, D.R., McCormick, T.L., Demetriades, N.W., Murphy, M.J., Holle, R.L., 2005. Lightning activity

related to satellite and radar observations of a mesoscale convective system over Texas on 7–8 April 2002. Atmos. Res. 76, 127–166.
Ferro, M.A.S., Saba, M.M.F., Pinto Jr., O., 2009. Continuing current in multiple channel cloud-to-ground lightning. Atmos. Res. 91, 399–403. http://dx.doi.org/10,1016/j.atmosres.2008.04.011.
Fleenor, S.A., Biagi, C.J., Cummins, K.L., Krider, E.P., Shao, X.M., 2009. Characteristics of cloud-to-ground lightning in warm-season thunderstorms in the Central Great Plains. Atmos. Res. 91, 333–352.
Georgis, J.-F., Roux, F., Chong, M., Pradier, S., 2003. Triple-Doppler radar analysis of the heavy rain event observed in the lago Maggiore region during MAP IOP2b. Q. J. R. Meteorol. Soc. 129, 495–522.
Houze Jr., R.A., 1997. Stratiform precipitation in regions of convection: a meteorological paradox? Bull. Am. Meteorol. Soc. 78, 2179–2196.
Houze Jr., R.A., Smull, B.F., Dodge, P., 1990. Mesoscale organization of springtime rainstorms in Oklahoma. Mon. Wea. Rev. 118, 613–654.
Krider, E.P., Musser, J.A., 1982. Maxwell currents under thunderstorms. J. Geophys. Res. 87, C13 (iC13p11171).
Lang, T.J., Rutledge, S.A., 2008. Kinematic, microphysical, and electrical aspects of an asymmetric bow-echo mesoscale convective system observed during STEPS 2000. J. Geophys. Res. 113, D08213. http://dx.doi.org/10.1029/2006JD007709.
Lang, T.J., Rutledge, S.A., Wiens, K.C., 2004. Origins of positive cloud-to-ground lightning flashes in the stratiform region of a mesoscale convective system. Geophys. Res. Lett. 31, L10105. http://dx.doi.org/10.1029/2004GL019823.
Livingston, J.M., Krider, E.P., 1978. Electric fields produced by Florida thunderstorms. J. Geophys. Res. 83 (C1), 385–401. http://dx.doi.org/10.1029/JC083iC01p00385.
MacGorman, D.R., Morgenstern, C.D., 1998. Some characteristics of cloud-to-ground lightning in mesoscale convective systems. J. Geophys. Res. 103 (D12), 14,011–14,024.
Marshall, T.C., Lin, B., 1992. Electricity in dying thunderstorms. J. Geophys. Res. 97, 9913–9918.
Marshall, J.S., Palmer, W.M., 1948. The distribution of raindrops with size. J. Meteorol. 5, 165–166.
Marshall, T.C., Rust, W.D., 1993. Two types of vertical electrical structures in stratiform precipitation regions of mesoscale convective systems. Bull. Am. Meteorol. Soc. 74, 2159–2170.
Marshall, T.C., Winn, W.P., 1982. Measurements of charged precipitation in a New Mexico thunderstorm: lower positive charge centers. J. Geophys. Res. 87, 7141–7157.
Mazur, V., Shao, X., Krehbiel, P.R., 1998. "Spider" lightning in intracloud and positive cloud-to-ground flashes. J. Geophys. Res. 103 (D16), 19,811–19,822.
Montanyà, J., Soula, S., Murphy, M., March, V., Aranguren, D., Solà, G., Romero, D., 2009. Estimation of charge neutralized by negative cloud-to-ground flashes in Catalonia thunderstorms. J. Electrost. 67 (2–3), 513–517 (May 2009).
Moore, C., Vonnegut, B., 1977. The thundercloud. In: Golde, R.H. (Ed.), Lightning. Physics of Lightning, vol. 1. Academic, San Diego, Calif, pp. 51–98.
Orville, R.E., Huffines, G.R., 1999. Lightning ground flash measurements over the contiguous United States: 1995–1997. Mon. Weather Rev. 127, 2693–2703.
Parker, M.D., Johnson, R.H., 2000. Organizational modes of midlatitude mesoscale convective systems. Mon. Weather Rev. 128, 3413–3436.
Parker, M.D., Rutledge, S.A., Johnson, R.H., 2001. Cloud-to-ground lightning in linear mesoscale convective systems. Mon. Weather Rev. 129, 1232–1242.
Petersen, W., Rutledge, S.A., 1992. Some characteristics of cloud-to-ground lightning in tropical northern Australia. J. Geophys. Res. 97 (D11), 11553–11560.
Rakov, V.A., Uman, M.A., Thottappillil, R., 1994. Review of lightning properties from electric field and TV observations. J. Geophys. Res. 99, 10,745–10,750. http://dx.doi.org/10.1029/93JD01205.
Ramsay, M.W., Chalmers, J.A., 1960. Measurement on the electricity of precipitation. Q. J. R. Meteorol. Soc. 86, 530–539.
Rutledge, S.A., Houze Jr., R.A., 1987. A diagnostic modeling study of the trailing stratiform region of a midlatitude squall line. J. Atmos. Sci. 44, 2640–2656.
Rutledge, S.A., MacGorman, D.R., 1988. Cloud-to-ground lightning activity in the 10–11 June 1985 Mesoscale Convective System observed during the Oklahoma–Kansas PRE-STORM project. Mon. Weather Rev. 116, 1393–1408.
Rutledge, S.A., Petersen, W.A., 1994. Vertical radar reflectivity structure and cloud-to-ground lightning in the stratiform region of MCSs: further evidence for in situ charging in the stratiform region. Mon. Weather Rev. 122, 1760–1776.
Rutledge, S.A., Lu, C., MacGorman, D.R., 1990. Positive cloud-to-ground lightning in mesoscale convective systems. J. Atmos. Sci. 47, 2085–2100.
Salek, M., Cheze, J.L., Handwerker, J., Delobbe, L., Uijlenhoet, R., 2004. Radar techniques for identifying precipitation type and estimating quantity of precipitation. European Cooperation in the Field of Scientific and Technical Research, Document of COST Action 717, WG 1, Task WG 1–2.
Schuur, T.J., Rutledge, S.A., 2000. Electrification of Stratiform regions in Mesoscale Convective Systems. Part II: Two-dimensional numerical model simulations of a symmetric MCS. J. Atmos. Sci. 57, 1983–2006.
Soula, S., 1994. Transfer of electrical space charge from corona between ground and thundercloud: measurement and modeling. J. Geophys. Res. 99 (D5), 10,759–10,765.
Soula, S., Chauzy, S., 1997. Charge transfer by precipitation between thundercloud and ground. J. Geophys. Res. 102, 11,061–11,069.
Soula, S., Chauzy, S., Chong, M., Coquillat, S., Georgis, J.-F., Seity, Y., Tabary, P., 2003. Surface precipitation current produced by convective rains during MAP. J. Geophys. Res. 108 (D13), 4395. http://dx.doi.org/10.1029/2001JD001588.
Standler, R.B., Winn, W.P., 1979. Effects of coronae on electric field beneath thunderstorms. Q. J. R. Meteorol. Soc. 105, 285–302.
Stolzenburg, M., Marshall, T.C., Rust, W.D., Smull, B.F., 1994. Horizontal distribution of electrical and meteorological conditions across the stratiform region of a mesoscale convective system. Mon. Weather Rev. 122, 1777–1797.
Stolzenburg, M., Rust, W.D., Marshall, T.C., 1998. Electrical structure in thunderstorm convective regions: 3. Synthesis. J. Geophys. Res. 103 (D12), 14,097–14,108. http://dx.doi.org/10.1029/97JD03545.
Wilson, C.T.R., 1929. Some thundercloud problems. J. Franklin Inst. 208, 1–12.